Robotica: (2019) volume 37, pp. 1415–1437. © Cambridge University Press 2019
doi:10.1017/S0263574719000031

Precision Grasp Planning for Multi-Finger Hand to Grasp Unknown Objects

Wenyu Yan†*, Zhen Deng‡, Jinbao Chen†, Hong Nie† and Jianwei Zhang‡

† *State Key Laboratory of Mechanics and Control of Mechanical Structures, Nanjing University of Aeronautics and Astronautics, Nanjing, China. E-mails: chenjbao@nuaa.edu.cn, hnie@nuaa.edu.cn*
‡ *TAMs, Department of Informatics, University Hamburg, Hamburg, Germany*
E-mails: deng@informatik.uni-hamburg.de, zhang@informatik.uni-hamburg.de

(Accepted January 1, 2019. First published online: February 21, 2019)

SUMMARY
Determining an appropriate grasp configuration for multi-finger grasping is difficult due to the complexity of robotic hands. The multi-finger grasp planning should consider not only geometry constraints of objects but also kinematics and dynamics of robotic hand. In this paper, a precision grasp-planning framework is presented for multi-finger hand to grasp unknown objects. First, the manipulation capabilities of the robotic hand are analyzed. The analysis results are further used as bases for the precision grasp planning. Second, the superquadric (SQ) fitting method is used for approximating unknown object models. Finally, a local–global optimization method is implemented to find appropriate grasp configurations for dexterous hand. The presented planning framework is validated in simulation experiments. Simulation results demonstrated that the presented grasp-planning framework enables the multi-finger hand to grasp unknown objects effectively.

KEYWORDS: Grasp Planning; Robotic hands; Pose Estimation and Registration; Optimization Robot Kinematics.

1. Introduction

Grasping with multi-finger hand is a popular topic in robotics, because it is an important part of the interaction between robot and environment. In order to grasp objects autonomously, a grasping strategy for unknown objects is essential to plan appropriate grasp configurations for robots. However, due to the high-dimensionality of grasping space and the uncertainty of the environment, grasp planning is a great challenge, especially for multi-finger hands. Typically, grasping is divided into power grasp and precision grasp.[1] Numerous researches for grasp planning have been studied based on these two aspects in the past few decades. Most researches mainly focus on power grasp, while precision grasp is rarely discussed. However, compared with power grasp, precision grasp has a wider application in daily manipulation and is a crucial factor to realize dexterous operation. Therefore, in this paper, our goal is to design an optimal precision grasp-planning framework for unknown objects by using multi-finger hand.

Recently, a number of precision grasp-planning methods have been proposed for multi-finger grasping. Most of these methods formulated the planning problem as a constrained optimization problem.[2–5] Because the constraint definitions are mainly based on object's geometry properties, most of these methods require an accurate object mesh model, which is difficult to be obtained in practical grasping application, and therefore limits these methods to known and familiar objects. In

* Corresponding author. E-mail: ywynuaa@163.com

https://doi.org/10.1017/S0263574719000031 Published online by Cambridge University Press

order to deal with unknown targets, some researches discussed generating grasp postures according to object's point cloud, but a known dataset of grasp postures is required.[6,7] Moreover, the characteristics of multi-fingered hand, such as manipulation capability, are not fully considered in previous methods. As grasp capabilities of robotic hands fundamentally depend on hand's mechanical structure, kinematics analysis of dexterous hand's mechanism will contribute to improve the efficiency of grasp syntheses.

To overcome the above shortages, a precision grasp-planning strategy for multi-finger hand to grasp unknown objects is proposed in this paper. An analysis of hand's manipulation capabilities is discussed firstly as a preprocess of planning. The detailed planning process includes two main steps: (1) representing object models based on superquadric (SQ) function[8–10] and (2) finding appropriate grasp configurations based on a local–global optimization algorithm. Compared with other researchers, the main contributions of our work are as follows:

1) A precision grasp-planning strategy is presented to discover grasp configurations for multi-finger hand to grasp unknown objects. This planning framework also takes manipulation properties of robotic hand into account.
2) An SQ fitting method is applied for object representation of precision grasp planning. Due to the compact formulation of SQ function, object surface features can also be calculated fast and directly during optimization.
3) A local–global optimization approach is presented to find a series of precision grasp configurations. Local properties of contact points, grasp stability and manipulation capabilities are considered comprehensively during the optimization.

The rest of this paper is organized as follows: In Section 2, the related works are reviewed. Section 3 introduces the proposed grasp-planning framework. The analysis results are discussed in Section 4. In Section 5, we conclude our work and introduce the future works.

2. Related Work

Grasp planning is a complex topic including lots of subproblems such as grasp stability analysis, grasp synthesis, object representation and so on.[11,12] Due to the complexity of the problem, most researches discussed about grasp planning based on power grasp. As a kind of reliable grasp with high capacity during interaction, sufficient grasp force and stability of power grasp are maintained by large contact area between the hand and objects. Therefore, most existing methods of power grasp planning mainly focus on the relative relation between the base frame of hand and objects.[13,14] Besides, in order to enhance the applicability to grasp unknown targets, lots of reconstruction methods are discussed,[14,15] among which SQ fitting is quite popular nowadays, because of its compact formulation and the ability to express a wide variety of objects with just a few parameters.[16–18]

Unlike power grasp, precision grasp only maintains contact points between fingertips and objects. The quality of grasping is largely influenced by the contact distribution. Considering disturbance resistance, force equilibrium and grasp stability, a variety of researches studied the relationship between contact distribution and grasp effectiveness.[19,20]A grasp quality measurement is proposed and widely used in precision grasp planning. This criterion, as well as contact force condition, is closely related to local surface properties of object. Therefore, an accurate object mesh model is required in most existing methods. Besides, corresponding to certain determined contact points, there are multiple configurations for pose of hand's base frame and angles of finger joints. Hence, precision grasp planning is normally formulated as a constrained optimization problem. Constraints are mainly established according to grasp quality measurement, and numerical optimization algorithm is usually used for solving the problem. However, in practical robotic grasping applications, object mesh models are always missing and the accurate contact points are hard to calculate. Some researches studied the segmentation of contact regions for fingertips based on object's point cloud.[6,21] Because of the lack of object's global information, the base frame of dexterous hand is hard to locate according to these discrete contact regions. A preestablished dataset of grasp configurations is required for the synthesis of precision grasp posture in this method.

https://doi.org/10.1017/S0263574719000031 Published online by Cambridge University Press

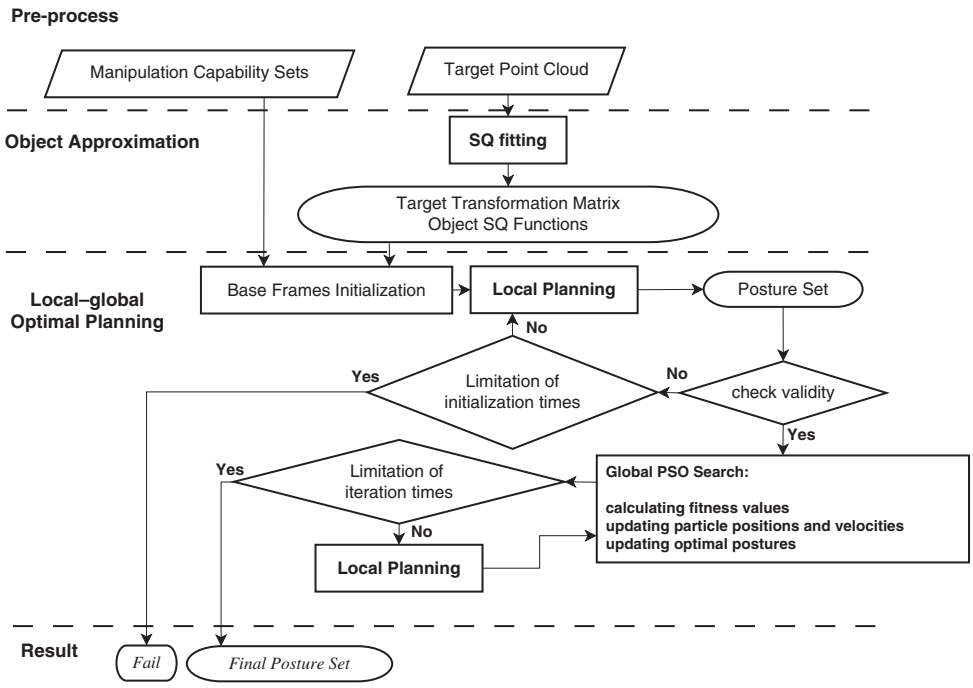


Fig. 1. The schematic of the precision grasp-planning framework.

In addition, as the general pre-grasping phase of in-hand manipulation, precision grasp partly determines the performance of subsequent operations. However, few researches have discussed the relationship between manipulation capability and grasp posture.[22] In this paper, we formulate the precision grasp planning as a constrained optimization problem combining the analysis of grasp stability and manipulation capabilities. SQ fitting is utilized for the approximation of unknown objects, as both global status and surface properties of objects can be obtained effectively with this method.

3. Methodology

This section presents a precision grasp-planning framework for a multi-fingered hand and the schematic is shown in Fig. 1. Manipulation capability analysis for dexterous hand is implemented as the preprocess and generates crucial planning parameters. SQ fitting and local–global optimization constitute the complete grasp-planning process. The detailed methods of this framework are discussed in the following subsections.

3.1. Manipulation capability analysis of robotic hand

Dexterous hand's structure influences the manipulation performance fundamentally. Analysis of manipulation capabilities helps to determine the feasible grasping space and reduce the complexity of grasp planning.

3.1.1. Characteristic analysis of human and robotic hand. A four-finger tendon-driven hand (FT-Hand) proposed in our previous work[23] is evaluated as an example in this paper. Hands with other structures can be evaluated by the similar method. The structure of the FT-Hand is shown in Fig. 2. This hand has 11 Degrees of Freedom in total. Index, middle and little fingers are defined as principal components analysis (PCA) fingers. Distal interphalangeal (DIP) joint and proximal interphalangeal (PIP) joint of PCA finger are coupled by a four-bar linkage. The metacarpophalangeal (MC) joint of the middle finger is fixed. The MC joints of the index and the little finger are coupled. Other joints of fingers are independent revolute joints. All the joints are driven by a pair of "tendon & spring." The driven system of tendons is placed in the forearm structure.[23] The frame of each phalanx is established based on Denavit–Hartenberg (DH) method. The base frame of the hand is set at the root of the middle finger as shown in Fig. 2(b). The geometry parameters of fingers are named as follows, for example: the phalanx length of the little finger are L_{l1}, L_{l2}, L_{l3}, L_{l4} from palm to

https://doi.org/10.1017/S0263574719000031 Published online by Cambridge University Press

Table I. The structure parameters of FT-Hand.

Parameter	**Value (mm)**	**Parameter**	**Value domain (°)**
L_{i1}, L_{t1}	8,0	θ_{i1}, θ_{t1}	[0,36],[0,110]
L_{i2}, L_{t2}	50,50	θ_{i2}, θ_{t2}	[0,90],[−60,60]
L_{i3}, L_{t3}	35,35	θ_{i3}, θ_{t3}	[0,100],−30,105]
L_{i4}, L_{t4}	25,25	θ_{t4}	[−30,105]

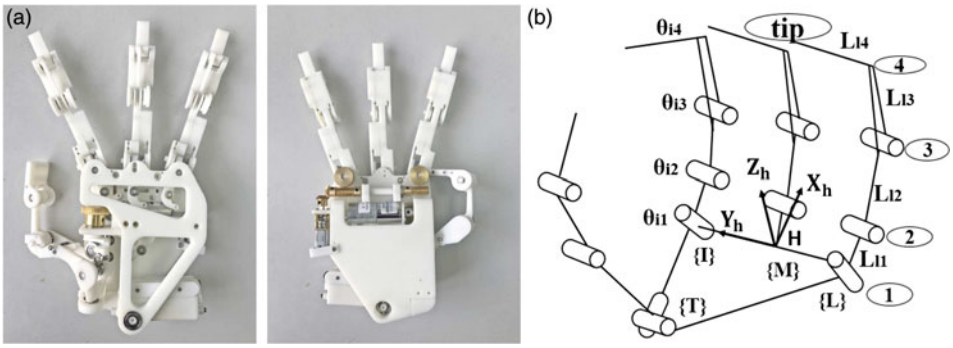


Fig. 2. A four-finger tendon-driven hand (FT-Hand).[23] (a) Hand prototype. (b) Sketch of the hand's structure. $\{H\}$ is the base frame of the hand and $\{I\}$, $\{M\}$, $\{L\}$, and$\{T\}$ are frames for index, middle, little and thumb fingers. The base frame origin of the hand coincides with the origin of $\{M\}$.

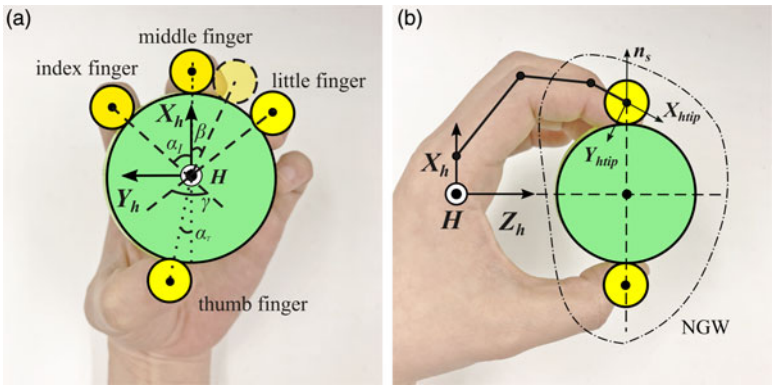


Fig. 3. Neutral configuration. (a) Grasp constraints in the X_h–Y_h plane. (b) Grasp constraints in the X_h–Z_h plane.

fingertip, and the joint angles of the index finger are $\Theta_i = (\theta_{i1},\ \theta_{i2},\ \theta_{i3},\ \theta_{i4})$ from palm to fingertip. The detailed structure parameters of FT-Hand are shown in Table I. The parameter values of other PCA fingers are set as the same as the index finger. The DIP and PIP joint angles of all PCA fingers follow the coupling relationship $\theta_{i4} = f_{\text{couple}}(\theta_{i3})$.

Human hand's grasping patterns are studied to develop evaluation methods and several characteristics are concluded as follows:

a. Human tends to grasp objects in neutral positions with relatively stable configurations as shown in Fig. 3. These grasp configurations are defined as neutral configurations for corresponding neutral positions.
b. Translation along the Y_h-axis is very small.
c. Grasp configurations can be synthesized by several manipulations from the neutral position.

Specific to the structure of FT-Hand discussed in this paper, objects cannot be translated along the Y_h-axis and displacement on the Y_h-axis can only be aroused by rotations, because the MC joint of the middle finger is fixed and the MC joints of the index and little fingers are coupled.

https://doi.org/10.1017/S0263574719000031 Published online by Cambridge University Press

3.1.2. Analysis of manipulation capabilities. Based on the above characteristic analysis of human and robotic hand, the hand's manipulation capabilities are evaluated from two aspects: the neutral graspable workspace (NGW) and the in-hand manipulation abilities (IMAs). The NGW is the collection of neutral positions, which is defined as a 2D region in the X_h–Z_h plane. The IMA are discussed based on the neutral configurations for the points within NGW, and are evaluated by achievable ranges of manipulations along three principal axes. During evaluation, sphere element objects are introduced to represent objects of different dimensions that may be handled in daily life.

- *Neutral graspable workspace*. The NGW for FT-Hand is a 2D region within the X_h–Z_h plane as shown in Fig. 3(b) and the grasp configurations for points outside the NGW is regarded as the combinations of in-hand manipulations. During the analysis, an object is placed at a discrete point in the X_h–Z_h plane, and the realizability of valid grasp configuration for the element object is checked at this point. A discrete point will be verified as valid if a valid configuration can be generated for the object at this point, as well as this configuration will be defined as the neutral configuration for this point. The NGW is the collection of all valid points. The detailed analysis is carried out according to the following two processes:

  (I) **Validity verification for grasp configuration**: The verification for grasp configuration is implemented by checking if there is a valid joint configuration for each finger. During verification, first the possible contact points P_{hobject} of fingertips on object's surface are calculated by exhaustion method, and then the joint angles of each finger are computed. To simplify the calculation, fingertips are modeled as spheres with 12 mm radius. All fingertips are limited in the plane, which simultaneously includes the object's center and keeps parallel to the X_h–Y_h plane as shown in Fig. 3(b). In addition, considering the contact stability, collision avoidance and force closure conditions, three constraints should be satisfied:

  (a) The angle between the Y_{htip}-axis of the fingertip's frame and the surface normal vector n_s at the contact point should be within [90°, 180°] as shown in Fig. 3(b).

  (b) The angle between the connections from any two fingertips to object center should be larger than $\beta = 2 * \arctan[r_{\text{fingertip}}/(r_{\text{fingertip}} + r_{\text{object}})]$ as shown in Fig. 3(a).

  (c) The fingertip of the thumb should be within angle γ as shown in Fig. 3(a).

$$\begin{cases} P_{\text{hobject}} = P_{hb} + [d, 0, 0],\ \alpha = 0 & \text{middle finger} \\ P_{\text{hobject}} = P_{hb} + [d\cos\alpha_I, d\sin\alpha_I, 0],\ \alpha = \alpha_I & \text{index finger} \\ P_{\text{hobject}} = P_{hb} + [-d\cos\alpha_T, d\sin\alpha_T, 0],\ \alpha = \alpha_T & \text{thumb} \\ d = r_{\text{fingertip}} + r_{\text{object}},\ \alpha_{T\max} = \max(\alpha_I, \pi - \alpha_I - \beta) \\ \alpha_I \in [\beta, \pi/2],\ \alpha_T \in [0, \alpha_{T\max}] \end{cases} \tag{1}$$

  According to above constraints, the possible contact point of each fingertip can be calculated as Eq. (1), where P_{hb} is the coordination of the object's center position. The pose of the little finger is symmetric to the index finger and its joint angles are $\Theta_l = (-\theta_{i1}, \theta_{i2}, \theta_{i3}, \theta_{i4})$. The calculation of finger joint configuration is modeled as a constrained optimization problem as Eq. (2), where $P_{\text{htip}}(\Theta)$ is the position of the fingertip. A discrete point will be verified as valid if the equations for all fingers have solutions.

$$\begin{cases} \min f(\Theta) = ((Y_{\text{htip}})_y/(Y_{\text{htip}})_x - \tan\alpha)^2 \\ s.t.\ (P_{\text{htip}}(\Theta) - P_{\text{hobject}}) < Tol_g,\ (X_{\text{tip}})_z > 0 \end{cases} \tag{2}$$

  (II) **Search strategy**: Because searching the valid points sequentially in open space produces numbers of invalid points, a row-major search strategy as shown in Fig. 4 is utilized in order to improve the computing efficiency. Initially, a wide search range is set. Then the search starts from a valid point $P_{h0} = [-14, 0, 73]$ which is determined by combining the individual workspace of each finger.[23] Row-search processes in two directions $\{+Z_h, -Z_h\}$ separately and repeats with a step offset on the X_h-axis after it reaches invalid points in both search directions. The search mode along the X_h-axis is defined as column-search as shown in Fig. 4. When no valid point exists within the entire row, the column-search will terminate. Because the initial point of row-search may locate outside the NGW, if the row-search starts with an

https://doi.org/10.1017/S0263574719000031 Published online by Cambridge University Press

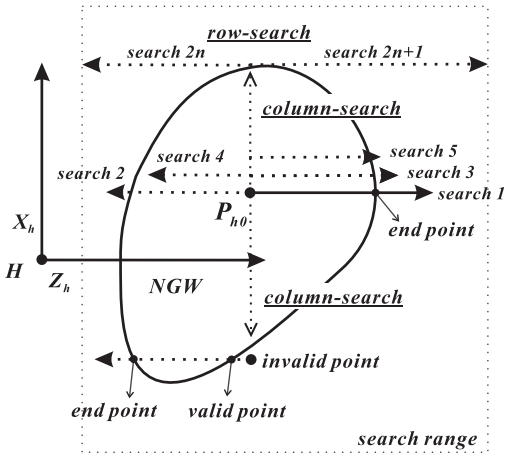


Fig. 4. The search strategy for the NGW.

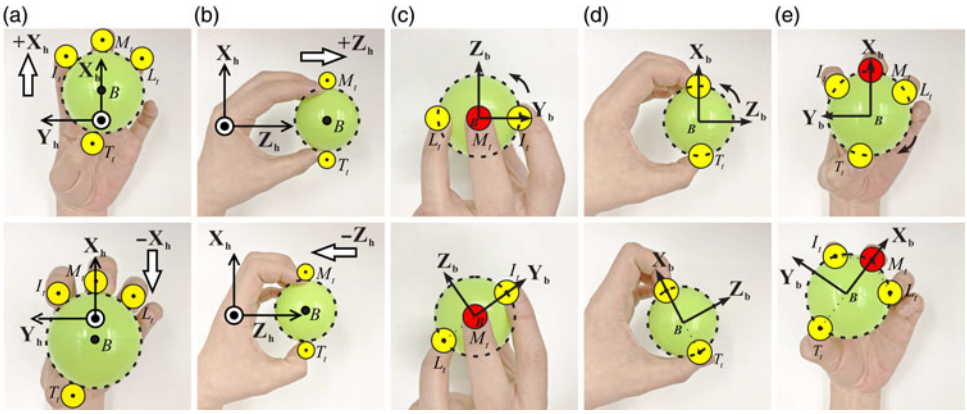


Fig. 5. In-hand translation and rotation. B is the center of the element object and I_t, M_t, L_t, and T_t are the tips of each finger. (a) Translation along the X_h-axis. (b) Translation along the Z_h-axis. (c) Rotation about the X_h-axis. M_t and T_t remain unchanged. (d) Rotation about the Y_h-axis. (e) Rotation about the Z_h-axis. M_t remains unchanged.

invalid point, the search will continue until the first invalid point comes after valid points. The detailed algorithm **WorkspaceSearching** is shown in Appendix A.

- *In-hand manipulation ability*. IMAs are divided into translations and rotations as shown in Fig. 5. The corresponding neutral configuration for each discrete point is the initial configuration of manipulation. Considering the continuity of manipulation, the relative positions of fingertips and object's center remain unchanged during motion. For translations, vectors $\overline{I_tB}$, $\overline{M_tB}$, $\overline{L_tB}$ and $\overline{T_tB}$ are constants, while for rotations these vectors rotate with the element object. For each manipulation ability estimation, the object is moved step by step from the neutral configuration and the target points of the fingertips change with $\overline{I_tB}$, $\overline{M_tB}$, $\overline{L_tB}$ and $\overline{T_tB}$ during the motion. Thus, the grasp verification for each step is formulated as follows:

$$\min g(\Theta) = (P_{\text{htip}}(\Theta) - P_{\text{hobject}})^2 \quad s.t.\ (X_{\text{tip}})_z > 0,\ g(\Theta) < Tol_m \tag{3}$$

The capability of a manipulation is defined as the largest motion range of the element object under this manipulation. The detailed algorithm **MotionRange** is shown in Appendix A. After the analysis of hand's manipulation capabilities, several evaluation sets can be obtained as planning parameters. The NGW is expressed as follows: $\mathbb{H}_G = \{(x_h, y_h, z_h) | y_h = 0, x_h \in \mathbb{H}_{Gx}, z_h \in \mathbb{H}_{Gz}\}$. The evaluation set of IMA is established to express the region of neutral positions with grasp configurations that have certain preferable manipulation capability. In this paper, the neutral configurations for the points within $\mathbb{H}_M = \{(x_h, y_h, z_h) | y_h = 0, x_h \in \mathbb{H}_{Mx}, z_h \in \mathbb{H}_{Mz}\}$ are supposed to have balanced manipulation capabilities in all direction and be suitable for grasping. Several evaluation sets of IMA

https://doi.org/10.1017/S0263574719000031 Published online by Cambridge University Press

can be established in advance to make the planning algorithm adaptive to different tasks. Therefore, all capabilities can be considered comprehensively to synthesis grasp configurations according to specific task requirements.

3.2. Object approximation based on SQ

In this paper, the SQ fitting method is used for object approximation and the SQ model expression is formulated as Eq. (4). The parameter vector $\overrightarrow{sp} = (a_1, a_2, a_3, \varepsilon_1, \varepsilon_2)$ incorporates all the parameters of SQ model, where ε_1, ε_2 control the shape of SQ model and a_1, a_2, a_3 express the size of SQ model in three main principle directions X_s, Y_s, Z_s. The local object frame $\{S\}$ is established at the center of SQ model. $F(\overrightarrow{sp} : x_s, y_s, z_s)$ is the "inside-outside" function. It is very convenient to judge the location of certain point. When $F = 1$, the point is on the surface of the model. If $F < 1$, the point lies inside the model. If $F > 1$, the point lies outside the model:

$$F(\overrightarrow{sp} : x_s, y_s, z_s) = \left(\left(\frac{x_s}{a_1} \right)^{\frac{2}{\varepsilon_2}} + \left(\frac{y_s}{a_2} \right)^{\frac{2}{\varepsilon_2}} \right)^{\frac{\varepsilon_2}{\varepsilon_1}} + \left(\frac{z_s}{a_3} \right)^{\frac{2}{\varepsilon_1}} \tag{4}$$

Because the SQ function as shown in Eq. (4) is established with respect to the SQ model center, the fitting result is sensitive to the coordinate of the object's center. In order to obtain a preferable fitting shape, the whole point cloud (x_g, y_g, z_g) of objects is gathered for the estimation of the object center (x_{gc}, y_{gc}, z_{gc}) in this paper. A rotation angle ϕ about the global Z_g-axis is also added in the function to fit the global pose of each object. Therefore, the transformation matrix of object can be defined as $T_{\text{gpose}}(x_{gc}, y_{gc}, z_{gc}, \phi)$. The object function of SQ fitting is formulated as Eq. (5) and the Levenberg–Marquardt method is utilized for calculation. This function is rewritten based on Eq. (4) in order to obtain a tight fitting model:[8,24]

$$\begin{cases} \min \sum (a_1^2 + a_2^2 + a_3^2)(F^{\varepsilon_1}(\overrightarrow{sp} : x_g - x_{gc}, y_g - y_{gc}, z_g - z_{gc}, \phi) - 1)^2 \\ s.t.\ \varepsilon_1, \varepsilon_2 \in [0.1, 1.9] \end{cases} \tag{5}$$

In addition, because SQ model is too regular to express the entire surface properties accurately, each point in the corresponding point cloud will be checked whether it locates near the surface of the object's SQ model after fitting. Points within a range near the surface are marked as inline points $\mathbb{S}_{in} = \{(x_g, y_g, z_g) || F(\overrightarrow{sp} : x_g - x_{gc}, y_g - y_{gc}, z_g - z_{gc}, \phi) - 1| < Tol_{in}\}$, which are utilized to value the planned grasp configuration in the next phase.

After fitting, the normal vector of each point on object's surface can be obtained by computing the gradient of the fitted SQ function at this point. Because parameters of SQ function all have explicit impacts on the model shape, by changing $\overrightarrow{sq}$, new SQ models can be shaped straightforward with relation to the fitted model. The SQ model can also be expressed as parametric equations shown in Eq. (6), where η, ω determine the location of point on the model's surface as shown in Fig. 6. Therefore, it is able to choose one point on the new SQ model, such as P_s in Fig. 6, with desired relation to the current object. The locating parameter vector (LP-Vector) can be defined as $\overrightarrow{lsp} = (a_1, a_2, a_3, \varepsilon_1, \varepsilon_2, \omega, \eta)$

$$\begin{cases} x(\overrightarrow{sp}, \eta, \omega) = a_1 \cos(\eta)^{\varepsilon_1} \cos(\omega)^{\varepsilon_2} \\ y(\overrightarrow{sp}, \eta, \omega) = a_2 \cos(\eta)^{\varepsilon_1} \sin(\omega)^{\varepsilon_2} \\ z(\overrightarrow{sp}, \eta, \omega) = a_3 \sin(\eta)^{\varepsilon_1} \\ \eta \in [-\pi/2, \pi/2], \ \omega \in [-\pi, \pi] \end{cases} \tag{6}$$

3.3. Precision grasp planning

This subsection introduces a precision grasp-planning approach based on a local–global optimization algorithm. Appropriate grasp configurations for objects subject to constraints are generated according to the results of previous analysis as shown in Table II.

https://doi.org/10.1017/S0263574719000031 Published online by Cambridge University Press

Table II. Pre-conditions of precise grasp planning.

Condition	**Detail**
NGW	$\mathbb{H}_G = \{(x_h, y_h, z_h) \vert y_h = 0, x_h \in \mathbb{H}_{Gx}, z_h \in \mathbb{H}_{Gz}\}^a$
IMA	$\mathbb{H}_M = \{(x_h, y_h, z_h) \vert y_h = 0, x_h \in \mathbb{H}_{Mx}, z_h \in \mathbb{H}_{Mz}\}^a$
Object information	1. Transformation matrix of object $T_{\text{gpose}}(x_{gc}, y_{gc}, z_{gc}, \phi)^b$
	2. SQ function of object $F(\overrightarrow{sp} : x_s, y_s, z_s, \phi) - 1 = 0^b$
	3. Parameter vector of the fitted SQ model $\overrightarrow{sp}_t = (a_{t1}, a_{t2}, a_{t3}, \varepsilon_{t1}, \varepsilon_{t2})^b$
Object's inline points set	$\mathbb{S}_{in} = \{(x_g, y_g, z_g) \vert \vert F(\overrightarrow{sp}_t : x_g - x_{gc}, y_g - y_{gc}, z_g - z_{gc}, \phi) - 1 \vert < Tol_{in}\}^b$

[a] $\mathbb{H}_G$ and $\mathbb{H}_M$ are specific to hand's base frame $\{H\}$.
[b] (x_s, y_s, z_s) is the coordinate in the SQ model frame. (x_g, y_g, z_g) and (x_{gc}, y_{gc}, z_{gc}) are the coordinates in the global frame.

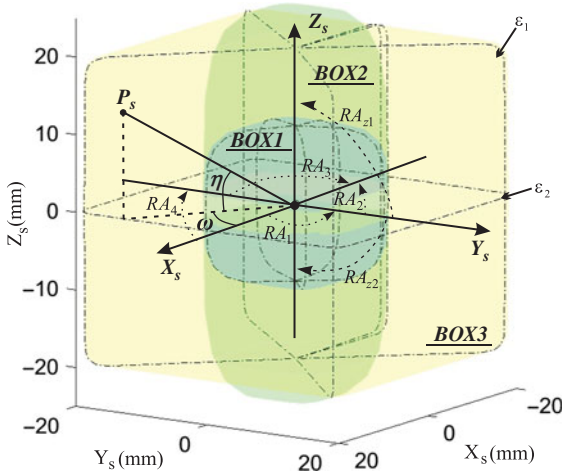


Fig. 6. The properties of parameters in SQ parametric equations. $\overrightarrow{sq}$ of three boxes: BOX1 $\overrightarrow{sq} =$ (10 mm, 10 mm, 10 mm, 0.5, 0.5); BOX2 $\overrightarrow{sq} =$ (10 mm, 10 mm, 20 mm, 0.5, 0.5); BOX3 $\overrightarrow{sq} =$ (20 mm, 20 mm, 20 mm,0.1, 0.1). $RA_1 : \omega \in [0, \pi/2]$, $RA_2 : \omega \in [\pi/2, \pi]$, $RA_3 : \omega \in [-\pi/2, -\pi]$, $RA_4 \in [0, -pi/2]$, $RA_{Z1} : \eta \in [0, \pi/2]$, $RA_{Z2} : \eta \in [0, -\pi/2]$.

3.3.1. Initialization of Hand's base frame. Grasp planning is aiming at generating feasible grasp configurations for objects and a reasonable feasible region is a key factor for the planning efficiency. In this paper, a feasible grasp region is utilized to limit the valid original points of hand's base frame. This region is determined according to the range of neutral positions in $\mathbb{H}_G$ and $\mathbb{H}_M$ as shown in Table II.

Normally, there are two general kinds of grasp modes for an object on the table as shown in Fig. 7(a). The Z_s-axis of the object frame is vertical to the table plane. In mode 1, the object is grasped from the top. In mode 2, the object is grasped from its lateral side. Because Z_h always points to the object, the distance range between the object's surface and the hand base frame equals the range of z_h in $\mathbb{H}_G$ as shown in Fig. 7(b). A tolerance Tol_{lb} is introduced to the lower bound to move the hand closer to the object center. The grasp mode 2 is infeasible for the object with small a_{t3}, which means these objects can be grasped only from the top. The limitation Tol_{a3} of a_{t3} is related to the dimension of the fingertip. The direction of the X_h-axis is determined by the shape parameter a_{t1} and a_{t2}. According to human's grasping pattern, people tend to grasp objects from the narrow side, which means, if $a_{t2} < a_{t1}$, the X_h-axis will point to the direction of the Y_s-axis as shown in Fig. 7(b). For the convenience of the following discussion, a_{t2} is assumed to be the smaller one. Therefore, the feasible region on the Y_s-axis is determined by the range of x_h in $\mathbb{H}_G$.

For the feasible grasp region, an upper bounding box and a lower bounding box, can be established according to above analysis as shown in Fig. 8. The parameter vectors of the lower bounding box $\overrightarrow{sp}_{lb} = (a_{lb1}, a_{lb2}, a_{lb3}, \varepsilon_{lb1}, \varepsilon_{lb2})$ and the upper bounding box $\overrightarrow{sp}_{ub} = (a_{ub1}, a_{ub2}, a_{ub3}, \varepsilon_{ub1}, \varepsilon_{ub2})$ are

https://doi.org/10.1017/S0263574719000031 Published online by Cambridge University Press

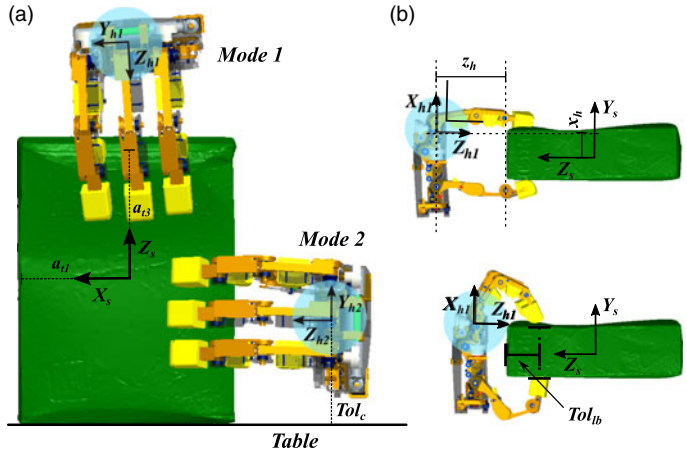


Fig. 7. Relative relations of the object and different grasp modes. (a) X_s–Z_s view. (b) Two ultimate grasp states.

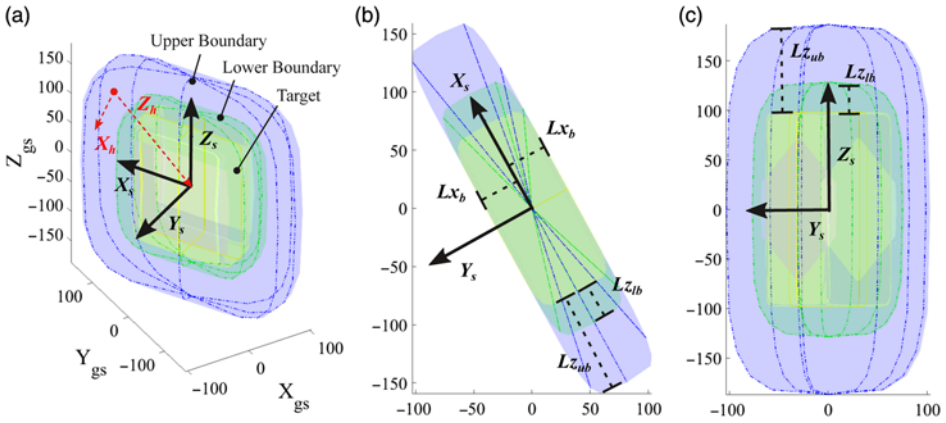


Fig. 8. Boundary of the feasible grasp region. The dot arrow line shows the establishment for the base frame on a stochastic initial point. X_{gs}, Y_{gs}, and Z_{gs} are three principle axes for the frame $\{GS\}$ established in the center of the SQ model but with the same orientation as the global frame.

formulated as follows:

$$\begin{cases} \overrightarrow{sp}_{lb} = (a_{t1},\, Lx_b,\, a_{t3} + Lz_{lb},\, \varepsilon_{t1},\, \varepsilon_{t2}) & a_{t3} \le Tol_{a3} \\ \overrightarrow{sp}_{ub} = (a_{t1},\, Lx_b,\, a_{t3} + Lz_{ub},\, \varepsilon_{t1},\, \varepsilon_{t2}) & \\ \overrightarrow{sp}_{lb} = (a_{t1} + Lz_{lb},\, Lx_b,\, a_{t3} + Lz_{lb},\, \varepsilon_{t1},\, \varepsilon_{t2}) & a_{t3} > Tol_{a3} \\ \overrightarrow{sp}_{ub} = (a_{t1} + Lz_{ub},\, Lx_b,\, a_{t3} + Lz_{ub},\, \varepsilon_{t1},\, \varepsilon_{t2}) & \end{cases} \tag{7}$$
$$Lz_{ub} = \{\max(z_h) | z_h \in \mathbb{H}_{Gz}\},\ Lz_{lb} = \{\min(z_h) - Tol_{lb} | z_h \in \mathbb{H}_{Gz}\}$$
$$Lx_b = \{\max(x_h) | x_h \in |\mathbb{H}_{Gx}|\}$$

The origins of a set of hand's base frames are generated randomly by the parametric equations as shown in Eq. (8). Two boundaries limit the ranges of the parameters in these equations. It should be noted that this bounding method will cause deviation of distance at corners, especially when ε_{t1} is small and the corner of the cross-section in the X_s–Z_s plane is very sharp. Therefore, if $\varepsilon_{t1} < 0.5$, both ε_{lb1} and ε_{ub1} are set to 0.5:

$$\begin{cases} x_{sh} = a_1 cos(\eta)^{\varepsilon_{t1}} cos(\omega)^{\varepsilon_{t2}} \\ y_{sh} = a_2 cos(\eta)^{\varepsilon_{t1}} sin(\omega)^{\varepsilon_{t2}} \\ z_{sh} = a_3 sin(\eta)^{\varepsilon_{t1}} \end{cases} \tag{8}$$
$$\forall a_1 \in [a_{lb1}, a_{ub1}],\ \forall a_2 \in [a_{lb2}, a_{ub2}],\ \forall a_3 \in [a_{lb3}, a_{ub3}]$$
$$\forall \omega \in [-\pi,\ \pi],\ \forall \eta \in [-\pi/2,\ \pi/2]$$

https://doi.org/10.1017/S0263574719000031 Published online by Cambridge University Press

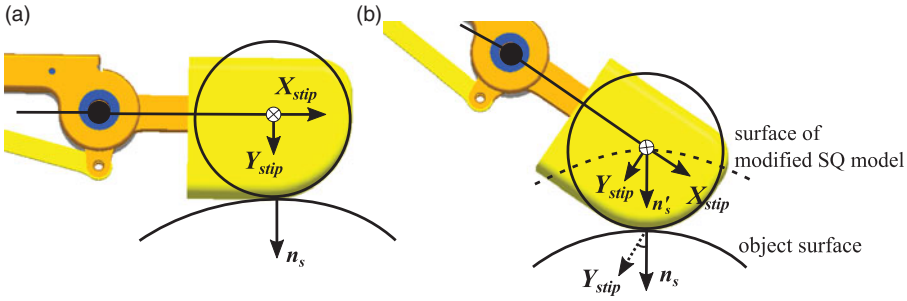


Fig. 9. Different contact conditions of the fingertip.

Because neutral positions within $\mathbb{H}_M$ are suitable for grasping, a preferable region can be delimited by the same method, and origins are generated in this field with higher probability. Besides, if obstacles exist, changing the values of η and ω can conveniently realize obstacle avoidance. For example, as shown in Fig. 7(a), the table is an obstacle. The distance between the origin of the hand's base frame and the table plane should be larger than Tol_c. This distance is checked for each initial base frame. If invalid, η will move a randomly step until the distance is larger than Tol_c.

Based on a settled origin (x_{sh}, y_{sh}, z_{sh}), three principle axes $\{X_h, Y_h, Z_h\}$ of the hand based frame are established by the following rules:

1) The vector from the hand's origin to the center of the object is Z_h as shown in Fig. 7(a). If $a_{t3} \leq Tol_{a3}$, $Z_h = -Z_s$.
2) $X_h = p_x V_{sh}$, where V_{sh} is the projection vector of the Y_s-axis in the plane vertical to Z_h-axis, and p_x is a correction parameter to modify the direction and calculated as Eq. (9). If $a_{t3} \leq Tol_{a3}$, X_h=$p_x Y_s$:

$$\begin{cases} p_x = sign[random(0,\,1) - 0.5] & y_{sh} \in \mathbb{H}_{Gx},\ -y_{sh} \in \mathbb{H}_{Gx} \\ p_x = sign(y_{sh}) & y_{sh} \in \mathbb{H}_{Gx},\ -y_{sh} \notin \mathbb{H}_{Gx} \\ p_x = -sign(y_{sh}) & y_{sh} \notin \mathbb{H}_{Gx},\ -y_{sh} \in \mathbb{H}_{Gx} \end{cases} \tag{9}$$

3) Y_h is established by the right-hand rule.

3.3.2. Grasp planning with local–global optimization. The proposed grasp planning is carried out based on a local–global optimization. The local optimization computes the joint configuration of each finger separately by optimizing the direction of fingertip's contact force. The particular precision grasp configuration is formed in this phase. The global optimization is proceeded by particle swarm optimization (PSO) algorithm to optimize the contact point distribution.

- *Local optimization phase.* A local grasp configuration is generated by planning for the four fingers separately with the given base frame. For each finger, the planning focuses on obtaining the valid joint angles with optimal contact condition of fingertip. As shown in Fig. 9(a), when the Y_{stip}-axis is in the same direction with the surface normal vector n_s, the contact area between the fingertip and the object's surface tends to be larger, therefore the contact stability will get better. The local optimization is formulated as Eq. (10), where PC_s are several points set on the hand's palm and phalanxes for collision avoidance detection.

  Because the accurate contact point on the surface is hard to calculate, n_s is replaced by a surface normal n'_s of a modified SQ model which goes through the fingertip center as shown in Fig. 9(b) and calculated as Eq. (11), where ${}^{\text{tip}}_{s}T(\Theta)$ is the transfer matrix from the fingertip's frame to the object's frame $\{S\}$, and $\overrightarrow{sp}_{fc} = (a_{t1} + r_{\text{fingertip}}, a_{t2} + r_{\text{fingertip}}, a_{t3} + r_{\text{fingertip}}, \varepsilon_{t1}, \varepsilon_{t2})$ is the parameter vector of the modified SQ model. In order to improve the computational efficiency, fingertip position is preplanned in the joint space. A close-boundary $\overrightarrow{sp}_{cb} = (a_{t1} + Tol, a_{t2} + Tol, a_{t3} + Tol, \varepsilon_{t1}, \varepsilon_{t2})$ is established by adding a tolerance to a_{t1}, a_{t2} and a_{t3}. The finger bends toward the surface of the object obeying the PCA-rule[23] until $F(\overrightarrow{sp}_{cb}; P_{\text{stip}}, \phi) - 1 < 0$. The joint angles of

https://doi.org/10.1017/S0263574719000031 Published online by Cambridge University Press

this state are utilized as the initial values:

$$\begin{cases} \min O(\Theta) = Y_{\text{stip}} \cdot n_s \\ s.t.\ (Y_{\text{stip}} \times n_s) \cdot Z_{\text{stip}} < 0,\ F(\overrightarrow{sp}_t : PC_s, \phi) - 1 > 0 \end{cases} \tag{10}$$

$$\begin{gathered} {}^{\text{tip}}_{s}T(\Theta) = \begin{bmatrix} X_{\text{stip}}(\Theta) & Y_{\text{stip}}(\Theta) & Z_{\text{stip}}(\Theta) & P_{\text{stip}}(\Theta) \\ 0 & 0 & 0 & 1 \end{bmatrix} \\ n_s = \nabla(F(\overrightarrow{sp}_{fc}; P_{\text{stip}}(\Theta), \phi) - 1) \end{gathered} \tag{11}$$

Powerful fingertip force may conflict with good manipulation capabilities, because the contact condition in Fig. 9(a) will make θ_4, θ_3 to be 0. Therefore, if good manipulation capabilities is the major purpose, the optimization equation should be reformulated. A distance constraint for $P_{\text{stip}}(\Theta)$ can be added into Eq. (10) according to $\mathbb{H}_M$.

- *Global optimization phase.* At the global search phase, the configurations with better contact distribution and grasp quality are determined. The search strategy used in this paper is PSO algorithm, which can expand the search scope based on both local and global optimum. The relative position between the hand's base frame and the object's center is set as the particle position, which is formulated as three position parameters $ppso = (ppso1, ppso2, ppso3)$ along the directions of three principal axes in the object frame as shown in the following equation:

$$\begin{cases} ppso1 = abs(z_{sh} - a_{t3}),\ ppso2 = abs(x_{sh}),\ ppso3 = abs(y_{sh}) & z_{sh} > a_{t3}\ mode\ 1 \\ ppso1 = abs(x_{sh} - a_{t1}),\ ppso2 = abs(z_{sh}),\ ppso3 = abs(y_{sh}) & z_{sh} \le a_{t3}\ mode\ 2 \end{cases} \tag{12}$$

The fitness value of each state is composed of two parts: (1) the overlap between the contact region and inline points and (2) the grasp quality generated by the traditional force-closure criterion.[19] For the first part, an inline point set $\mathbb{S}_{in}$ is established after fitting, and it is necessary to ensure all the contact points located in this point set. The traditional way to judge the inclusion relation is to check the number of the inline points within a circle r_{tip} around the contact point. However, because objects have different dimensions and point cloud densities, it is hard to set a unified criterion for all objects. Therefore, a dimensionless overlap ratio σ_r by normalizing the point numbers of four fingertips is utilized instead. If inline points distribute evenly around all contact points of a grasp configuration, all fingertips of this configuration are regarded as located in the overlapped region. Otherwise, the fingertip with the lower ratio may locate outside. The minimum ratio value of the configuration is returned as the fitness value. For the second part, the criteria Q_∞[19] is utilized for the grasp quality evaluation. The grasp quality values should also be normalized, in order to gather all the fitness indices together. Therefore, the maximum values of the grasp quality in the first PSO iteration are utilized as the reference parameters for normalization. If the new particle locates outside the feasible region, the fitness value will be set to 0 directly.

Because PSO searching is hard to converge to a certain global optimal state for grasp-planning problem, the termination of the search is set to be the end of iterations. The detailed **PSOSearching** algorithm is shown in Algorithm 1.

The integrated framework of the local–global optimal planning method is shown in Fig. 10. The local planning has two main effects: (1) to initialize a set of postures for the global PSO search and (2) to synthesize postures for particle positions. All the detailed hand postures, including configurations of all joint angles, are generated by the local optimization algorithm. The global planning focuses on the relative position between the hand's base frame and the object. The location of the base frame is designed as the particle position. The fitness value consists of the grasp quality Q_∞ and the overlap ratio σ_r. The position of the hand's base frame will be updated during each iteration of PSO search and finally converge to several optimal regions. When the hand's base frame locates within these regions, the postures generated by the local planning will be more possible to have high Q_∞ and σ_r.

4. Evaluation Results and Simulation

The detailed results of the manipulation capability analysis are presented in this section. Based on the evaluation sets generated from the analysis, simulations are conducted to validate the proposed

https://doi.org/10.1017/S0263574719000031 Published online by Cambridge University Press

Algorithm 1: PSOSearching

Input: Object's SQ parameter vector $\overrightarrow{sp}_t$, $\mathbb{S}_{in}$ and transformation matrix T_{gpose}
Output: Configuration Set $G_{configuration} = [G_g, G_p]$

begin
  Initialization: partical number *pnum*, iteration times *iternum*, initialization limitaion *ininum*, global index $gindex = 0$, partical index $pindex = \emptyset$, $G_{configuration}$=$\emptyset$, $bframe = \emptyset$, particale velocities $pvec = (pvec1, pvec2, pvec3)$, particale positions *ppos*;
  for $il = 1$ **to** *ininum* **do**
    hframe=BaseframeInitialization($\overrightarrow{sp}_t$, *pnum*);
    Pset=LocalPlan(*hframe*, $\overrightarrow{sp}_t$);
    if $Pset \neq \emptyset$ **then** break;
  if *Pset*=$\emptyset$ **then** Error("Fail Initialization"), **return**;
  Initialize the particle's best known position: $Pset \rightarrow G_p$, *ppso*;
  for $ip = 1$ **to** *pnum* **do**
    `/* inp is the number of overlapped inline points */`
    inp=CheckInline(*Pset*, $\mathbb{S}_{in}$, T_{gpose}) σ_r=$r1[ip]$=min(*inp*/ max(*inp*));
    $r2[ip]$=Force(P_{tip},$\overrightarrow{sp}_t$, T_{st}); $r3[ip]$=Moment(P_{tip},$\overrightarrow{sp}_t$, T_{st}); `// grasp quality`
  $pr2 = \max(r2)$; $pr3 = \max(r3)$; $pindex = r1 + r2/pr2 + r3/pr3$;
  Update the Swarm's best known position G_g, *gindex*;
  Update particle velocities and positions *pvec*, *ppso*;
  for $ig = 1$ **to** *iternum* **do**
    hframe=NewFrame(*ppso*); *Pset*=LocalPlan(*hframe*, $\overrightarrow{sp}_t$);
    for $ip = 1$ **to** *pnum* **do**
      Calculate the fitness value r;
      if $r > G_p[ip]$ **then**
        update $pindex[ip]$, $G_p[ip]$;
        if $r > gindex$ **then** update *gindex*, G_g;
      Update particle velocities and positions *pvec*, *ppso*;

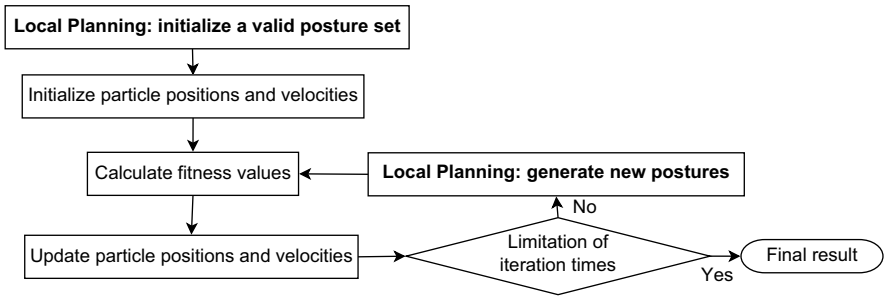


Fig. 10. The framework of the local–global optimal planning

planning methods, including SQ fitting and local–global optimization. To test the proposed grasping planning strategy, a collaborative simulation is carried out based on ROS Indigo and Matlab R2015b. The test objects are selected from the YCB dataset.[25]

4.1. Results and discussion of manipulation capability analysis

In this paper, balls with 15 mm, 20 mm, 25 mm, 30 mm, 35 mm and 40 mm radius are chosen as element objects for the analysis of hand's manipulation capabilities. These balls represent not only spherical objects but also objects with similar local dimensions.

The NGWs of FT-Hand for different element objects are shown in Fig. 11. Figure 12 shows the IMA of grasp configurations for two element objects with radius = 15 35 mm. The analysis results

https://doi.org/10.1017/S0263574719000031 Published online by Cambridge University Press

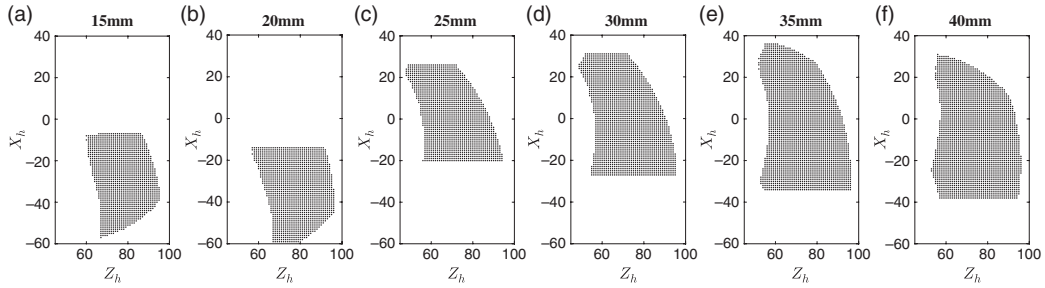


Fig. 11. The NGW of FT-Hand for different element objects, radius = 15 mm, 20 mm, 25 mm, 30 mm, 35 mm and 40 mm. The unit of X_h- and Z_h-axis is millimeter.

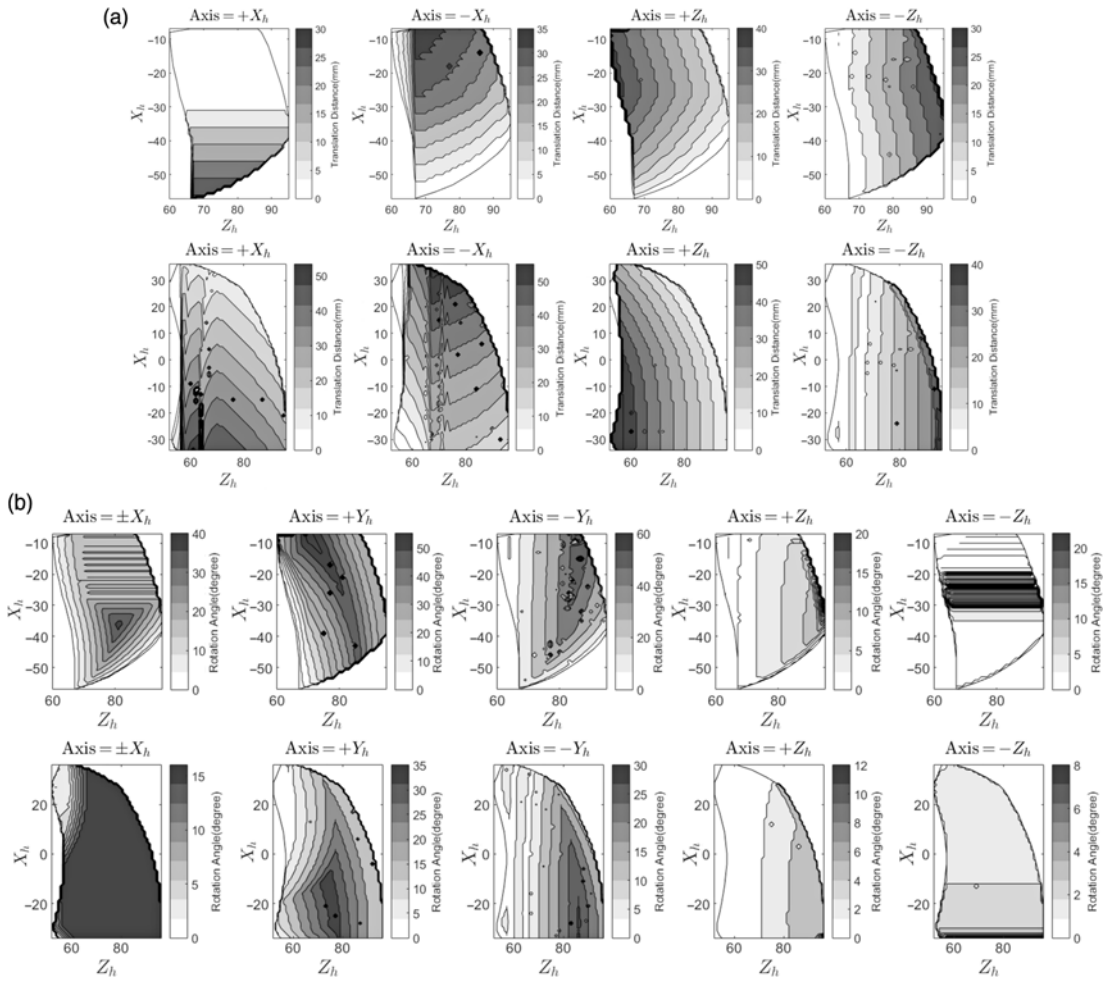


Fig. 12. In-hand manipulation ability of grasp configurations for the element objects. The unit of the X_h- and the Z_h-axis is millimeter. (a) Translation abilities: radius = 15 mm, radius = 35 mm. (b) Rotation abilities: radius = 15 mm, radius = 35 mm.

for other element objects are shown in Appendix B. According to the results, for objects with different dimensions, FT-Hand shows two general kinds of manipulation properties. Correspondingly, the element object is divided into two groups: objects with radius ≤ 20 mm are defined as S-object and others are defined as L-object.

- *Evaluation results of NGW*. As shown in Fig. 11, the NGWs of FT-Hand for all element objects locate in the range (50, 100) on Z_h-axis, but differ on X_h-axis. The NGWs of S-object locate only on the $-X_h$-axis, while for L-object, the NGWs distribute in the similar regions on the

https://doi.org/10.1017/S0263574719000031 Published online by Cambridge University Press

$+X_h$- and the $-X_h$-axis. This difference is caused by the mechanical structure of FT-Hand. When index and little finger have no lateral rotation θ_{i1}, $\theta_{l1} = 0$, the PCA fingers cannot all contact with the small radius objects at the same time, because fingertips will hinder with each other. To grasp small objects, the index and little fingers must bend largely and simultaneously rotate laterally, which will move the region of valid points toward $-X_h$ direction and lead to larger lateral rotation angles of these two fingers for grasping S-objects than for L-objects. As shown in Fig. 11, for S-object, the NGW locates within the space $\mathbb{H}_{GS} = \{(x_h, y_h, z_h)|y_h = 0, x_h \in (-60, 0)\text{ mm}, z_h \in (50, 100)\text{ mm}\}$, while for L-object, the NGW locates within the space $\mathbb{H}_{GL} = \{(x_h, y_h, z_h)|y_h = 0, x_h \in (-40, 40)\text{ mm}, z_h \in (50, 100)\text{ mm}\}$.

- *Evaluation results of IMA*. For different points in NGW, the achievable manipulation range of the corresponding neutral configuration is different as shown in Fig. 12. Therefore, the best grasp configuration varies with particular manipulation tasks. The large lateral rotation angles of index and middle finger to grasp S-objects also cause two distinguishing features of IMA:

  1) For the points $\{(x_h, z_h)|x_h \in (-30, 0)\text{ mm}\}$ in S-object's NGW, the translation manipulation of the corresponding neutral configurations performs poorly in the $+X_h$ direction.
  2) Neutral configurations for S-object have good performance in rotation about the Z_h-axis, while configurations for L-object perform poorly in rotation about the Z_h-axis.

  In general, for S-objects, neutral configurations in the range $\mathbb{H}_{MS} = \{(x_h, y_h, z_h)|y_h = 0, x_h \in (-25, -35)\text{ mm}, z_h \in (70, 80)\text{ mm}\}$ has balanced IMA in all direction. For L-objects, the range is $\mathbb{H}_{ML} = \{(x_h, y_h, z_h)|y_h = 0, x_h \in (-5, 5)\text{ mm}, z_h \in (70, 80)\text{ mm}\}$.

According to the discussion above, NGW $\mathbb{H}_G$ differs with object's dimension, and in-hand manipulation capabilities relate to the locations of the neutral configurations in NGW. The center region $\mathbb{H}_M$ of NGW has balanced manipulation performance. During simulation experiments, the detailed set is chosen according to the object's dimension. If $a_{t1} \leq 20\,\text{mm}$, $\mathbb{H}_G = \mathbb{H}_{GS}$, $\mathbb{H}_M = \mathbb{H}_{MS}$, else $\mathbb{H}_G = \mathbb{H}_{GL}$, $\mathbb{H}_M = \mathbb{H}_{ML}$.

4.2. Results and discussion of SQ fitting

During the simulation, the point clouds of objects are gathered in a scene built up in Gazebo 2.2. This scene includes a table, two Kinects, and an object. These Kinects are set on two opposite sides of the table separately. The global frame $\{G\}$ is built up at the center of the table and the Z_g-axis is vertical to the table plane. At the beginning of each simulation, an object is randomly put into the scene. Then the point cloud of the scene is gathered by Kinects and Gaussian noise is added to the gathered signal. After modifying the whole point cloud based on Point Cloud Library (PCL), the point cloud of the object is obtained and utilized as the input for our planning framework. Figure 13 shows some examples of SQ fitting. For the unknown object with rough convex shape, SQ fitting performs effectively for model representation.

During the fitting process, the transfer matrix $T_{\text{gpose}}(x_{gc}, y_{gc}, z_{gc}, \phi)$ and surface information of the object can be obtained simultaneously. In order to judge the local property approximation performance of SQ fitting, Figs. 13 and 14 show the estimation results of surface normal vectors at inline points by SQ function and PCL library, respectively. For each object, the average normal orientation error $\Delta\theta_n$ is calculated. According to the comparison, several conclusions can be concluded as follows:

1. The estimation deviation $\Delta\theta_n$ for objects with regular shapes are acceptable as shown in Fig. 14. However, if the inline point locates on the edge of the fitted SQ shape, the surface normal calculated by SQ function is normally incorrect, especially for box-like and columnar shapes. For objects with all dimensions smaller than 20 mm, the SQ function performs more stable than PCL library in estimation. Because during the extraction of object point cloud from the signal of the Kinect, normally a supervoxel filter is performed for the whole original point cloud at first. This step aims to speed up the computation, however it will cause the deficiency of the points in the small object point cloud, which leads to the inaccuracy of surface normal estimation by the general method in PCL library.

https://doi.org/10.1017/S0263574719000031 Published online by Cambridge University Press

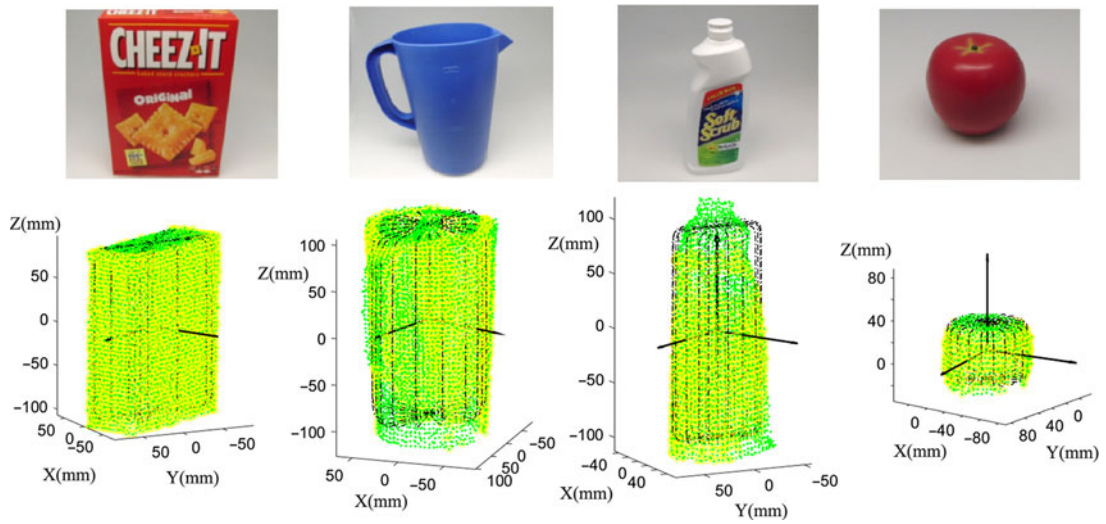


Fig. 13. SQ fitting results for objects from the YCB set. The green points are the original points and the yellow points are the inline points. The transfer matrix for the objects is $T_{\text{gpose}}(x_{gc}, y_{gc}, z_{gc}, \phi)$.

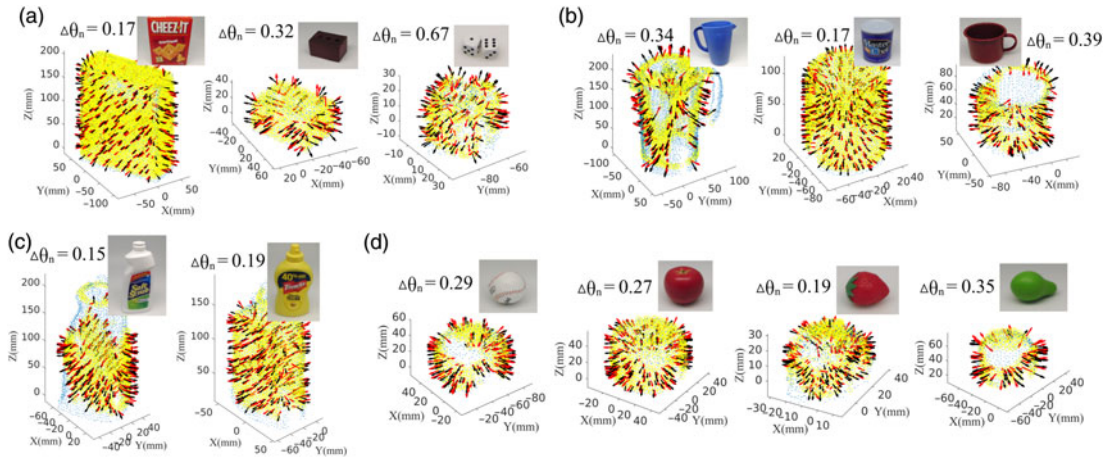


Fig. 14. Normal estimation for objects with regular shape. The black arrows are surface normals calculated by SQ functions. The red arrows are surface normals estimated by PCL library. The unit of θ_n is radian. (a) Boxes. (b) Cylinders. (c) Elliptical cylinders. (d) Balls

2. For ball-like objects, the general estimation errors $\Delta\theta_n$ are relatively larger. Because during the collection of object point cloud, the bottom part of ball-like object will be sheltered by the upside, which leads to the incomplete of point cloud and the large deviation for the object's center estimation. Therefore, the errors of fitted SQ shapes and estimated normal vectors for ball-like objects are slightly larger than other objects as shown in Fig. 14(d).
3. For flat objects with very small size in Z-dimension, SQ function performs very poorly in surface normal estimation, which is also caused by inaccurate object's centers.
4. For objects with irregular shapes, SQ fitting results are improper. A method combining segmentation and SQ modeling can be utilized to improve fitting results[9] as shown in Fig. 15(b). The subpart with large dimensions or many inline points is chosen as the main part for the planning of contact locations.

It has to be mentioned, that $\Delta\theta_n$ cannot directly indicate the quality of normal estimation, because both methods have errors. The SQ function can only be utilized for estimations of surface normals at inline points, and estimation errors increase at the edge of SQ shapes. Surface normal vectors generated by SQ method reflect the general surface properties, but perform weakly in the expression of very detailed features. The common normal vector estimation method in PCL library performs

https://doi.org/10.1017/S0263574719000031 Published online by Cambridge University Press

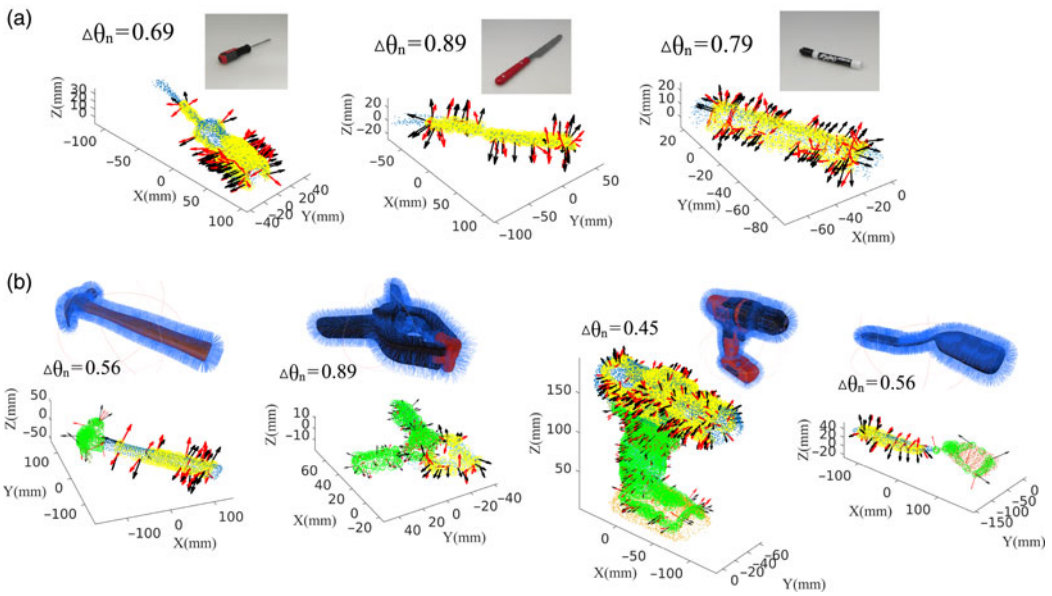


Fig. 15. Normal estimation for objects with special shape. The black arrows are surface normals calculated by SQ functions. The red arrows are surface normals estimated by PCL library. The unit of θ_n is radian. (a) Shapes with small dimensions in Z-axis (b) Complex shapes. The first row of figures for complex shapes show the results estimated within the software MeshLab V1.3.2.

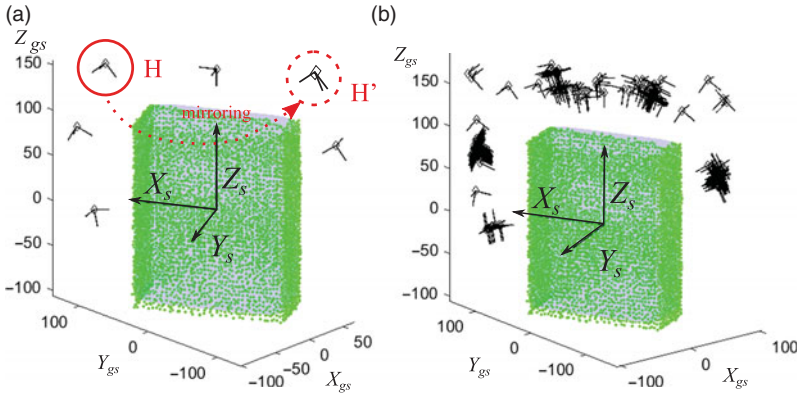


Fig. 16. PSO searching process. The unit of axes is millimeter. (a) Initial particles. (b) Terminal state of PSO searching.

well in the presentation of local features, but sometimes it is too precise for surface textures. For example, for surfaces covered with anti-skid rubber particles, too detailed normal vector estimation is an obstacle to grasp planning. Besides, deficiency of points in the target point cloud will also cause the instability of normal vector accuracy.

As discussed above, a fitting quality evaluation index E_{sq} formulated as Eq. (13) should be calculated after SQ fitting. If $E_{sq} < Tol_{sq}$, SQ fitting combining point cloud segmentation will be done to improve the fitting quality.[9] In this paper, Tol_{sq} is set to be 0.55:

$$E_{sq} = \frac{number\ of\ the\ points\ in\ \mathbb{S}_{in}}{number\ of\ the\ points\ in\ the\ original\ point\ cloud} \tag{13}$$

4.3. Results and discussion of precision grasp planning

In the simulation, the local planning is used for configuration synthesis during each revolution of PSO search. For PSO, the number of iteration is set to 100, the learning factors are set to 1 and the time factor is formulated as $\omega = 1 - ig/iteration$. Five particles are initialized for PSO as shown in Fig. 16, and five final configurations for a box-like object are shown in Fig. 17.

https://doi.org/10.1017/S0263574719000031 Published online by Cambridge University Press

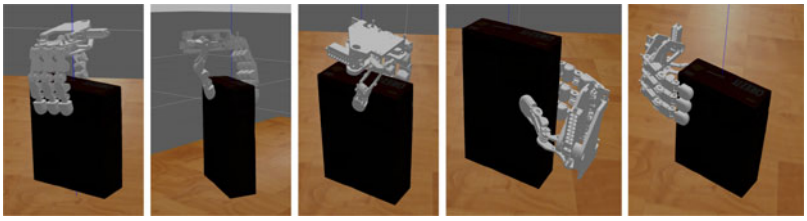


Fig. 17. The grasp configurations for the box-like object.

Table III. Grasping success ratios for different objects.

Object	**Ratio**	**Object**	**Ratio**
Large bottle	0.90	Apple	0.95
Small bottle	0.93	Pear	0.90
Large cup	0.85	Drill	0.90
Small cup	0.55	Screwdriver	0.95
		Hammer	0.95

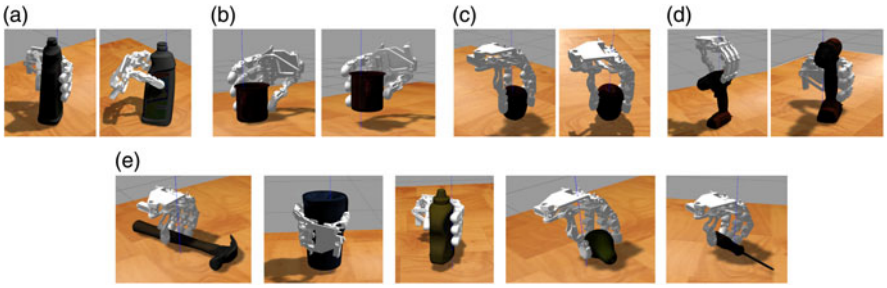


Fig. 18. Grasp configurations for different targets. (a) Large bottle. (b) Small cup. (c) Apple. (d) Drill. (e) Hammer, large cup, small bottle, pear and screwdriver.

This planning framework generates several valid grasp configurations together with their evaluation indices for unknown objects with different dimensions, even for small dices. The local planning costs most of the planning time, because it includes a traditional optimization process. In order to enhance the computation speed, the number of particles should be limited below 10, but the small number of particles may cause the global PSO search converge to the local optimum. Therefore, a mirror probability is introduced into the global search. The origin of hand's base frame within the region $\{(x_{sh}, y_{sh}, z_{sh})|z_{sh} < 0\}$ has a possibility to be mirrored about the $X_s - Y_s$ plane, while the origins within the region $\{(x_{sh}, y_{sh}, z_{sh})|z_{sh} > a_{t3}\}$ may be mirrored about the $Z_s - Y_s$ plane as shown in Fig. 16(a). This mirror operation makes the searching process expand more efficiently to the whole range of the feasible region with fewer particles and iterations.

For the initial particles, two conditions need to be satisfied according to the simulation results:

1. At least one valid configuration should be included in the initial particles, otherwise, the search will diverge and exceed the feasible region very fast.
2. More initial particles should be set for small objects, because feasible grasp configurations for small object are very limited. If the initial particles is too few, configuration synthesis will fail at most PSO search positions. Increasing the number of initial particles will not reduce the computation speed, because point clouds of small objects include fewer points, so that SQ fitting and local planning processes will be more efficient than large objects.

More objects are tested in the simulation environment as shown in Fig. 18. During the simulation, weights of all objects are set to be 100g. We execute 30 trials on each object, and the success ratios for all objects are shown in Table III. Because of the inaccuracy of fitted SQ model edges, if there

https://doi.org/10.1017/S0263574719000031 Published online by Cambridge University Press

are important surface features near this region, the success ratio of grasp planning will be largely reduced, such as small cup shown in Fig. 17(b).

The local–global optimization planning method introduced in this paper is effective for regular and convex shapes. For objects with irregular features, the planning method has different performances:

1) Object has concave or special local geometry on the surface, such as the bottles shown in Fig. 14(c): Although SQ models are regular and convex shapes, several irregular local geometries on the surface will not interfere with the grasp planning. The contact points will only locate within the overlap region between the fitted model and the original point cloud. This is the importance to import the inline point set S_{in} into the global optimization.
2) Object's shape is complex, such as the drill and clamp shown in Fig. 15(b), or concave, such as banana or crescent: If the fitting quality $E_{sq} < Tol_{sq}$, a method combining segmentation and SQ modeling is utilized for these objects to improve fitting results. The original point clouds of objects is segmented into several subparts, and SQ fitting is executed for each subpart. Therefore, the final SQ model for the original object may consist of several submodels. A submodel with better fitting quality is chosen as the main part for grasp planning, while other submodels are regarded as obstacles.
3) Object with important local features, such as mug with a handle or annulus: Because fitted SQ model is the envelope shape of object, local features inside the SQ model is hard to express. Therefore, with the local–global planning method, the contact points will never locate on those local features. However, this does not mean that the planning method cannot generate a valid posture. The contact points of those valid postures can still locate on the envelope shape. Taking a mug as an example, by the presented planning method, the robotic hand will not grasp the handle, but the main body of the mug.

As a conclusion, the proposed local–global optimization planning method is able to generate valid postures for irregular objects, but the successful ratio of grasping is lower than regular objects.

Compared with other researches for grasp planning, SQ fitting is utilized for precise grasp planning in this paper, which is rarely discussed before. The planning framework introduced in this paper is able to deal with unknown objects without precalculated posture sets. Besides, it can generate several poses of the hand's base frame and relevant configurations of all joints at the same time.

5. Conclusion

In this paper, to stably grasp unknown objects by multi-finger hand, an optimal precision grasp-planning strategy is presented. The manipulation capabilities of the robotic hand are analyzed first. The analysis results are utilized as the pre-conditions of the planning algorithm to increase the efficiency. Second, an SQ fitting method is utilized for reconstructing object models, which enables the proposed grasp planning to deal with unknown object. Inline points are extracted to represent feasible grasp region. Particularly for complex objects, a method combining segmentation and SQ fitting was utilized instead. Thirdly, in order to find an appropriate grasp configuration, a local–global optimization method is applied. The contact optimization for each fingertip generates the local grasp configuration and the PSO search algorithm is used for determining the grasp configuration with better contact distribution. Finally, simulations are implemented to demonstrate the proposed grasp-planning framework.

The proposed grasp-planning framework is suitable for grasping unknown objects. However, its planning efficiency is not high enough to realize online planning. Improving the efficiency will be our primary future work. At the same time, in order to realize the proposed grasp-planning framework on a real-world platform, the allocation of finger contact force and unified hand-arm planning are also considered in our future work.

Acknowledgments

This work was supported by the National Natural Science Foundation of China [grant number 51675264] and the German Science Foundation (DFG) and National Science Foundation of China (NSFC) in project Crossmodal Learning under contract Sonder-forschungsbereich Transregio 169.

https://doi.org/10.1017/S0263574719000031 Published online by Cambridge University Press

References

1. M. R. Cutkosky, "On grasp choice, grasp models, and the design of hands for manufacturing tasks," *IEEE Trans. Robot. Autom.* **5**(3), 269–279 (1989).
2. N. Vahrenkamp, L. Westkamp, N. Yamanobe, E. E. Aksoy and T. Asfour, "Part-Based Grasp Planning for Familiar Objects," *Proceedings of the IEEE/RAS International Conference on Humanoid Robots,* Cancun, Mexico (2016), pp. 919–925.
3. P. Song, Z. Fu and L. Liu, "Grasp planning via hand-object geometric fitting," *Vis. Comput.* **3**(4), 1–16 (2016).
4. M. T. Ciocarlie and P. K. Allen, "Hand posture subspaces for dexterous robotic grasping," *Int. J. Robot. Res.* **28**(7), 851–867 (2009).
5. H. A. Bunis, E. D. Rimon, Y. Golan and A. Shapiro, "Caging polygonal objects using equilateral three-finger hands," *IEEE Robot. Autom. Lett.* **2**(3), 1672–1679 (2017).
6. K. Hang, M. Li, J. A. Stork, Y. Bekiroglu, F. T. Pokorny, A. Billard and D. Kragic, "Hierarchical fingertip space: A unified framework for grasp planning and in-hand grasp adaptation," *IEEE Trans. Robot.* **32**(4), 960–972 (2016).
7. T. Osa, J. Peters and G. Neumann, "Experiments with Hierarchical Reinforcement Learning of Multiple Grasping Policies," *Proceedings of the International Symposium on Experimental Robotics,* Roppongi, Tokyo (2016), pp. 160–172.
8. A. Jaklic, A. Leonardis and F. Solina, "Segmentation and recovery of superquadrics," *Comput. Imaging Vis.* **20** (2000).
9. L. Chevalier, B. Nautibus, F. Jaillet and A. Baskurt, "Segmentation and superquadric modeling of 3D Objects," *J. WSCG* **11**(1) (2003).
10. K. Duncan, S. Sarkar, R. Alqasemi and R. Dubey, "Multi-Scale Superquadric Fitting for Efficient Shape and Pose Recovery of Unknown Objects," *Proceedings of the IEEE International Conference on Robotics and Automation,* Karlsruhe, Germany (2013), pp. 4238–4243.
11. J. Bohg, A. Morales, T. Asfour and D. Kragic, "Data-driven grasp synthesis: A survey," *IEEE Trans. Robot.* **30**(2), 289–309 (2013).
12. A. Sahbani, S. El-Khoury and P. Bidaud, "An overview of 3D object grasp synthesis algorithms," *Robot. Autonom. Sys.* **60(3)**, 326–336 (2012).
13. I. Gori, U. Pattacini, V. Tikhanoff and G. Metta, "Ranking the Good Points: A Comprehensive Method for Humanoid Robots to Grasp Unknown Objects," *Proceedings of the International Conference on Advanced Robotics,* Sydney, Australia (2013), pp. 1–7.
14. Z. C. Marton, L. Goron, R. B. Rusu and M. Beetz, "Reconstruction and verification of 3d object models for grasping," *Robotics Research*. Springer (2011), pp. 315–328.
15. N. Blodow, R. B. Rusu, Z. C. Marton and M. Beetz, "Partial View Modeling and Validation in 3D Laser Scans for Grasping," *Proceedings of the 9th IEEE-RAS International Conference on Humanoid Robots,* Paris, France (2009), pp. 459–464.
16. G. Vezzani, U. Pattacini and L. Natale, "A Grasping Approach Based on Superquadric Models," *Proceedings of the IEEE International Conference on Robotics and Automation,* Singapore (2017), pp. 1579–1586.
17. A. Makhal, F. Thomas and A. P. Gracia, "Grasping Unknown Objects in Clutter by Superquadric Representation," *2018 Second IEEE International Conference on Robotic Computing (IRC)*, Laguna Hills, CA, USA (2018) pp. 292–299.
18. C. Goldfeder, P. K. Allen, C. Lackner and R. Pelossof, "Grasp Planning via Decomposition Trees," *Proceedings of the IEEE International Conference on Robotics and Automation,* Roma, Italy (2007), pp. 4679–4684.
19. C. Ferrari and J. Canny, "Planning Optimal Grasps," *Proceedings of the IEEE International Conference on Robotics and Automation,* Nice, France (1992), pp. 2290–2295.
20. F. T. Pokorny and D. Kragic, "Classical Grasp Quality Evaluation: New Algorithms and Theory," *Proceedings of the IEEE/RSJ International Conference on Intelligent Robots and Systems,* Tokyo, Japan (2013), pp. 3493–3500.
21. M. A. Roa and R. Suarez, "Computation of independent contact regions for grasping 3D objects," *IEEE Trans. Robot.* **25**(4), 839–850 (2009).
22. M. A. Roa, Z. Chen, I. C. Staal, J. N. Muirhead and A. Maier, "Toward a Functional Evaluation of Maniplation Performance in Dexterous Robotics Hand Design." *Proceedings of the IEEE International Conference on Robotics and Automation,* Hong Kong, China (2014), pp. 6800–6807.
23. W. Yan, H. Nie, J. Chen and D. Han, "Optimal design and grasp ability evaluation of four-finger tendon-driven hand," *Int. J. Adv. Robot. Syst.* **14**(6), (2017). doi: 10.1177/1729881417748444
24. F. Solina and R. Bajcsy, "Recovery of parametric models from range images: The case for superquadrics with global deformations," *IEEE Trans. Pattern Anal. Mach. Intel.* **12**(2), 131–147 (1990).
25. B. Calli, A. Walsman, A. Singh, S. Srinivasa, P. Abbeel and A. M. Dollar, "Benchmarking in manipulation research: Using the Yale-CMU-Berkeley object and model set," *IEEE Robot. Automat. Mag.* **22**(3), 36–52 (2015).

https://doi.org/10.1017/S0263574719000031 Published online by Cambridge University Press

Appendix A

Algorithm 2: WorkspaceSearching

Input: $P_0 = [-14, 0, 73]$, radius of the element object r, β, search step Δp, search range z_{up}, z_{low}, x_{up}, x_{low}

Output: Point set R_p, finger joint angles set J

```
1  begin
2      i = 0, R = ∅, J = ∅;
3      for x_i = 1 to x_up;                                   // column-search
4       do
5          flag = 1;
6          for z_i = 1 to z_up;                               // line-search
7           do
8              check the validity of P_i;
9              if P_i is valid then
10                 P_i → R_p, finger joints angles Θ_n → J, P_{i+1} = P_i + [0, 0, Δp],
                     i = i + 1, flag = 0
11             else
12                 if flag ≠ 0 then P_{i+1} = P_i + [0, 0, Δp], i = i + 1;
13                 else break;
14         flag = 1, P_i[3] = 72;
15         for z_i = 1 to z_low;                              // line-search
16          do
17             check the validity of P_i;
18             if P_i is valid then
19                 P_i → R_p, Θ_n → J, P_{i+1} = P_i − [0, 0, Δp], i = i + 1, flag = 0
20             else
21                 if flag ≠ 0 then P_{i+1} = P_i − [0, 0, Δp], i = i + 1;
22                 else break;
23         if flag == 1 then break;
24         else P_i[3] = 73, P_{i+1} = P_i + [Δp, 0, 0], i = i + 1;
25     P_i = [−15, 0, 73];
26     for x_i = 1 to x_low do
27         same as line5 to line22;
28         if flag == 1 then break;
29         else P_i[3] = 73, P_{i+1} = P_i − [Δp, 0, 0], i = i + 1;
```

https://doi.org/10.1017/S0263574719000031 Published online by Cambridge University Press

Algorithm 3: MotionRange

Input: Neutral point set R, finger joint angles set J, motion step set S
Output: Motion range set M

begin
  $num = Size(R)$, $M = \emptyset$;
  for $ip = 1$ **to** num **do**
    $P_0 = R_p[ip]$, $\Theta_n = J[ip]$, $P_0 \rightarrow M$;
    /* P_0 is the element object center */
    $[Pf_{tt},\ Pf_{it},\ Pf_{mt},\ Pf_{lt}] = ForwardKinematics(\Theta_n)$;
    /* Coordination of each fingertip */
    $Vb_t = Pf_{tt} - P_0$, $Vb_i = Pf_{it} - P_0$, $Vb_m = Pf_{mt} - P_0$, $Vb_l = Pf_{lt} - P_0$;
    for $id = 1$ **to** 8 **do**
      /* translation directions including $+X_h$, $-X_h$, $+Z_h$, $-Z_h$ */
      /* rotation directions including $+X_h$, $+Y_h$, $-Y_h$, $-Z_h$ */
      $flag = 1$, $i = 1$, P_r, $P_i = P_0$, $rot = 0$;
      while $flag == 1$ **do**
        if $id \leq 4$ **then**
          /* for translations */
          $P_{i+1} = P_i + S[id]$;
          $Pf_t = Vb_t + P_{i+1}$, $Pf_i = Vb_i + P_{i+1}$, $Pf_m = Vb_m + P_{i+1}$;
          CheckValidation(Pf_t, Pf_i, Pf_m);
          if *invalid* **then** $i - 1 \rightarrow M$, $flag = 0$;
          $i = i + 1$;
        else
          $rot = rot + S[id]$, $M_{trans} = \text{TransMatrix}(rot)$;
          if $id == 8$ **then** $P_r = M_{trans} * (-Vb_m) + P_{mt}$;
          /* rotation around Z_h-axis is specific to M_t */
          $Pf_t = M_{trans} * Vb_t + P_r$, $Pf_i = M_{trans} * Vb_i + P_r$,
          $Pf_m = M_{trans} * Vb_m + P_r$, $Pf_l = M_{trans} * Vb_l + P_r$;
          CheckValidation(Pf_t, Pf_i, Pf_m, Pf_l);
          if *invalid* **then** $rot - S[id] \rightarrow M$, $flag = 0$;

https://doi.org/10.1017/S0263574719000031 Published online by Cambridge University Press

Appendix B

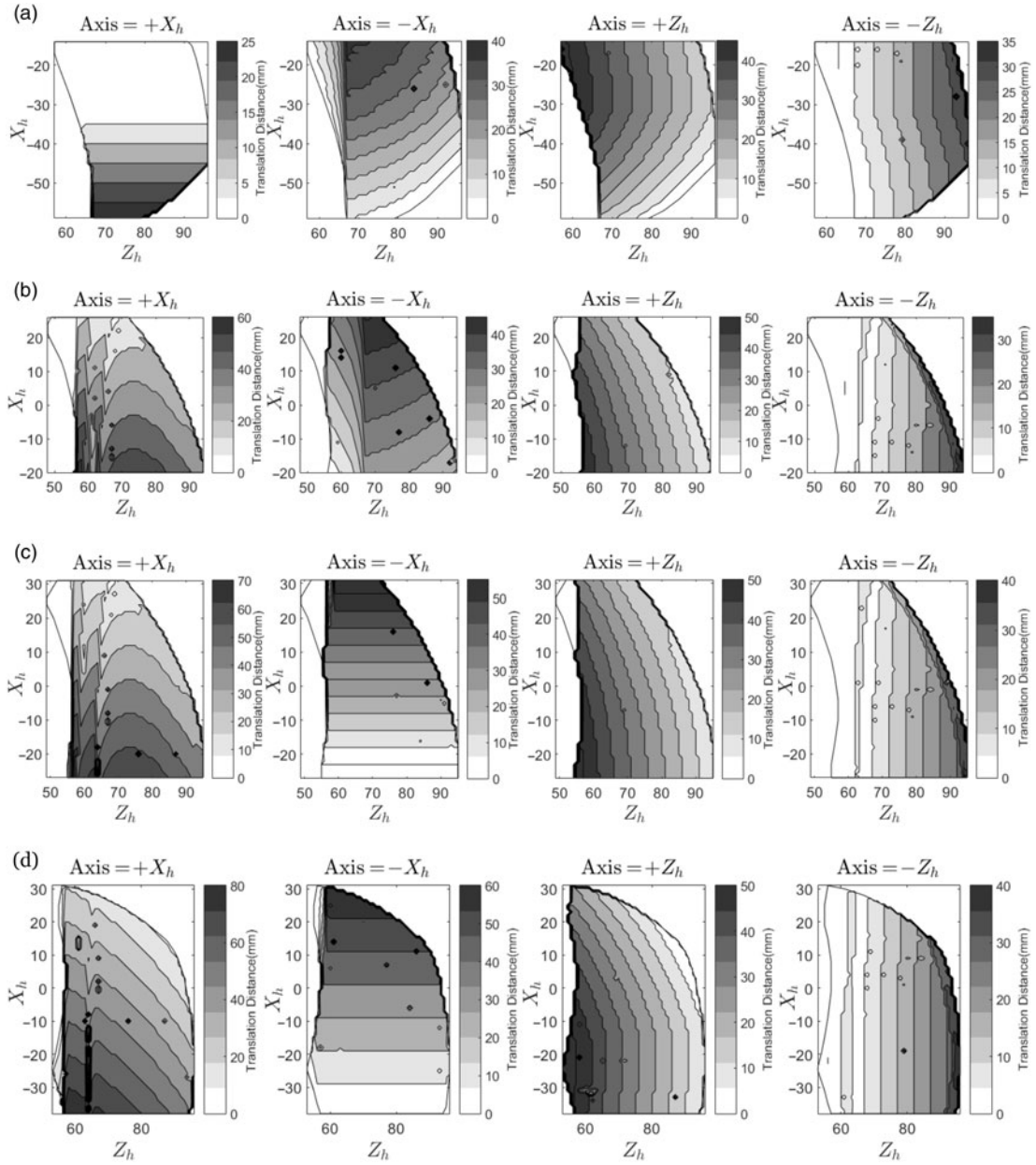


Fig. 19. Translation capability of FT-Hand for element objects. The unit of X_h and Z_h is millimeter. (a) Radius = 20 mm, (b) radius = 25 mm, (c) radius = 30 mm and (d) radius = 40 mm.

https://doi.org/10.1017/S0263574719000031 Published online by Cambridge University Press

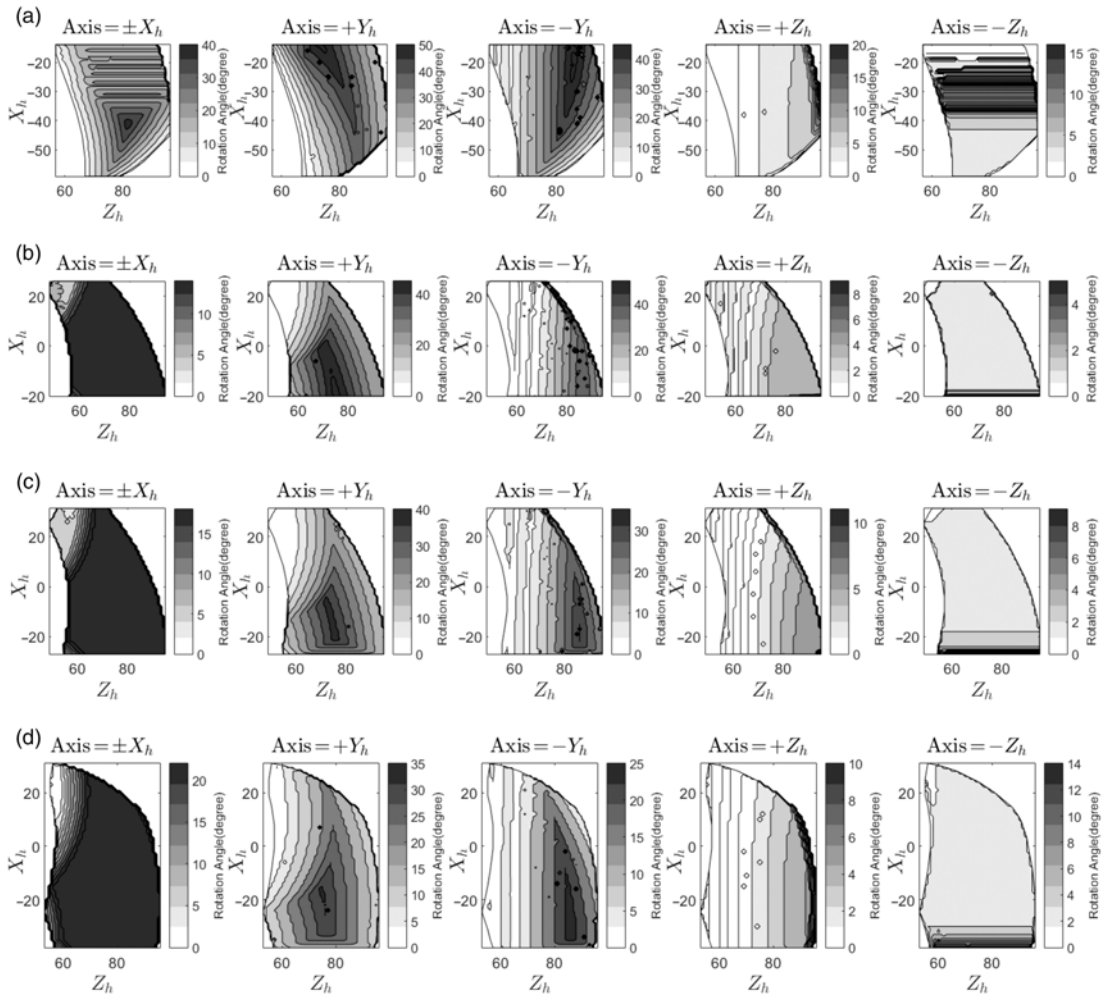


Fig. 20. Rotation capability of FT-Hand for element objects. The unit of X_h and Z_h is millimeter. (a) Radius = 20 mm, (b) radius = 25 mm, (c) radius = 30 mm and (d) radius = 40 mm.

https://doi.org/10.1017/S0263574719000031 Published online by Cambridge University Press